J. Phys. D: Appl. Phys. **33** (2000) R1–R16. Printed in the UK PII: S0022-3727(00)04626-X

REVIEW ARTICLE

Property variation with shape in magnetic nanoelements

R P Cowburn

Nanoscale Science Group, Department of Engineering, University of Cambridge, Trumpington Street, Cambridge CB2 1PZ, UK

Received 9 September 1999

Abstract. Nanometre scale magnetic particles ('nanoelements' or 'nanomagnets') form a rich and rapidly growing new area in condensed matter physics, with many potential applications in data storage technology and magnetic field sensing. This paper reviews an extensive study into the influence of shape on the properties of nanomagnets in the size range 35–500 nm. Elliptical, triangular, square, pentagonal and circular geometries have all been considered. It is shown that the size, thickness and geometric shape of nanomagnets all play a vital role in determining the magnetic properties. The shape, size and thickness of a nanomagnet are shown to be linked to its magnetic properties by two distinct phenomena. The first is called configurational anisotropy and describes the role played by small deviations from uniformity in the magnetization field within the nanostructures, which allow unexpected higher-order anisotropy terms to appear. These anisotropies can often dominate the magnetic properties. The second is the competition which exists between exchange energy and magnetostatic energy. This competition determines whether the nanomagnets exhibit single domain or incoherent magnetization and also controls the non-uniformities in magnetization which lead to configurational anisotropy. Understanding the influence of shape opens the way to designing new nanostructured magnetic materials where the magnetic properties can be tailored to a particular application with a very high degree of precision.

1. Introduction

One of the most exciting recent developments in magnetism has been the use of nanometre fabrication techniques to form nanometre scale magnets. These so-called nanomagnets, or nanoelements, possess by virtue of their extremely small size very different magnetic properties from their parent bulk material. Interest in the study of these fascinating particles has been driven undoubtedly by the success of the semiconductor microelectronics industry, in four different ways. First, demand for magnetic hard disk data storage has grown commensurately with the spread and increase in the capabilities of microcomputers. Hard disks store their data as sub-micrometre scale magnetic domains. A detailed understanding of magnetism on the nanometre scale is therefore essential for developing new hard disks. Moreover, it is generally thought that the current growth in performance of hard disks (60–100% per annum compound increase in storage density) can only be sustained into the future if the hard disk itself is replaced by a massive array of magnetic nanoelements [1]. Second, the art and science of fabricating structures on the nanometre scale have benefited from the exponential shrinking in size of the integrated circuit transistor [2], leading to enormous investment in optical and electron beam lithography. Third, the mathematical equations governing magnetic behaviour on the nanometre scale are highly nonlinear and can generally only be studied theoretically using computer-intensive numerical algorithms [3] (although, see as an exception [4]). The recent increase in availability of low-cost, high-power processors has now enabled nanomagnetism to become a widely studied branch of condensed matter theory. Fourth, the semiconductor industry may itself in the future benefit from nanomagnetism. Many of the problems currently facing future reduction in size of integrated circuits, such as the diminishing number of carriers present in a transistor gate and difficulties in removing heat, may be solved by combining magnetic elements into microchips [5]. In the first instance this will probably be in the form of non-volatile computer memory called MRAM (magnetic random access memory) and process control microchips with built-in magnetic sensors for the automotive industry. The recent discovery [6] of how to inject spin polarized current from a ferromagnet into a semiconductor now means that in the future we may see fully hybrid magnetic–electronic devices which use the spin of the electrons as much as their charge to perform logic operations and processing. Nanomagnets may ultimately even provide a suitable environment for implementing quantum computation [7].

A further, more fundamental motivation for studying nanomagnets comes from the history of magnetics research. While physicists have long recognised that reducing a lengthscale is the natural way to study magnetism, experimental techniques only reached a sufficiently advanced

0022-3727/00/010001+16$30.00

stage of development in the 1950s, enabling foundational work to be performed by Prutton and others [8]. The arrival of molecular beam epitaxy in the laboratory during the 1980s allowed monolayer thickness magnetic films of high structural quality to be routinely grown, leading to much research during the 1980s and 1990s into two-dimensional magnetic systems [9]. A number of exciting new phenomena such as oscillatory exchange coupling [10], giant magneto-resistance [11] and perpendicular surface anisotropy [12] were discovered during this rich period, all associated in some way with the fact that the film thickness had been reduced to the nanometre regime. The next thing to do was, naturally, to apply this principle to the other two dimensions. One-dimensional magnetism has thus been studied in magnetic wires [13] and zero-dimensional magnetism, in which all three dimensions are structured in the nanometre lengthscale, is currently one of the fastest growing fields in condensed matter physics.

The most important property of a naturally occurring magnetic element or alloy is its anisotropy. This refers to the presence of preferred magnetization directions within the material and is, ultimately, responsible for determining the way in which a magnetic material behaves and the technological applications for which it is suitable. In a conventional magnetic material, anisotropy arises from the shape and symmetry of the electronic Fermi surface and so is intrinsic to the particular element or alloy and cannot easily be tailored. In nanomagnets, however, the anisotropy depends not only on the band structure of the parent material, but also on the *shape* of the nanomagnet. One of the most attractive features of nanostructured magnetic materials, therefore, is that their magnetic properties can be engineered by the choice of the shape of the constituent nanomagnets.

The most widely studied shape of nanomagnet to date has been rectangular, due largely to the applicability of such structures to MRAM and spin-valve magnetic field sensors [14]. A number of experimental [15] and theoretical [16] studies have been conducted. Several other studies have investigated circular magnetic elements with either in-plane or out-of-plane magnetization [17], this time often with an eye to patterned media for ultra-high density hard disk data storage. A smaller number of workers have looked at square nanoelements [18]. None of these studies, however, has systematically compared the influence of different shapes. In this paper we review an extensive comparative study which we have performed into the influence of shape and size on the magnetic properties of nanostructures. We have made small arrays of magnetic nanostructures on a silicon substrate using high-resolution electron beam lithography. The nanomagnets were in the size range 35–500 nm and in the thickness range 3–15 nm and had elliptical, triangular, square, pentagonal and circular geometries, which respectively correspond to rotational symmetries of order 2, 3, 4, 5 and ∞. The parent material was Supermalloy ($Ni_{80}Fe_{14}Mo_5X_1$ where X is other metals), which we chose because in bulk, it is almost isotropic and so any anisotropy in the nanomagnets must come from their shape. A high-sensitivity magneto-optical method was then used to probe the magnetic properties of these nanomagnets. We show that the geometric shape of the nanomagnets plays a key role in determining their magnetic properties in two distinct ways. The first is through a new phenomenon called configurational anisotropy, in which very small deviations of the magnetization from uniformity can couple to the shape of the particle. The second way comes as a result of the shape of the particle stabilizing or destabilizing the single domain state.

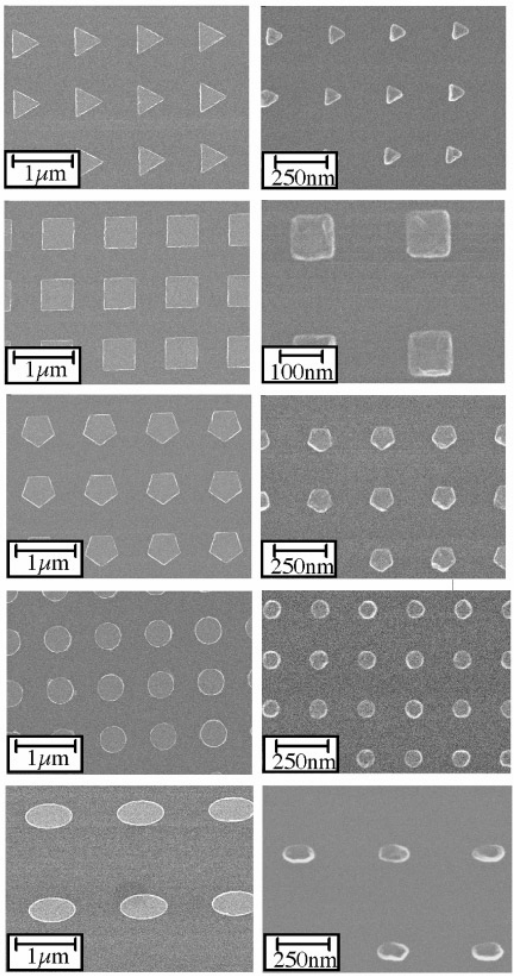

Figure 1. SEM images of some of the nanomagnets fabricated during this study. The sizes are 500 nm (left-hand column) and <100 nm (right-hand column).

This paper is structured as follows. Section 2 describes the experimental and theoretical methods which we used during the course of our study. Section 3 then describes the properties which we have observed in elliptical nanomagnets (section 3.1), triangular, square and pentagonal nanomagnets (section 3.2), isolated circular nanomagnets (section 3.3) and finally interacting circular nanomagnets arranged on a rectangular lattice (section 3.4). Important common themes are discussed in section 4, followed by a conclusion in section 5.

2. Experimental and theoretical methods

2.1. Nanomagnet fabrication and characterization

All of the samples were made using high-resolution electron beam lithography with a standard lift-off pattern transfer

process [19]. Two layers of polymethylmethacrylate (PMMA), one of molecular weight 495 000 and one of weight 950 000, were spun onto a single crystal silicon substrate. Arrays of different geometric shapes were then exposed onto the sample in a Jeol 4000EX SEM/TEM operating at 100 kV, followed by 30 s of development in a 1:3 solution of methyl iso-butyl ketone/iso-propyl alcohol. The array size was between (5 μm)^2 and (10 μm)^2; the spacing between each nanomagnet was usually at least equal to the diameter of the nanomagnet, and for the smallest structures was usually as large as three times the diameter. This ensured that there was negligible magnetostatic interaction between nanomagnets. A 3–15 nm thick layer of $Ni_{80}Fe_{14}Mo_5$ ('Supermalloy') followed, in most cases by a 5 nm thick anti-oxidation capping layer of gold were then deposited at a rate of 0.08 nm s^{-1} by electron beam evaporation in an ultra-high vacuum chamber with base pressure 4×10^{-9} mbar. An unpatterned substrate was also present in the chamber to allow structural and magnetic characterization of the unpatterned magnetic film. Ultra-sonic assisted lift-off in acetone was used to remove the magnetic film from the unexposed parts of the patterned sample.

Transmission electron microscopy (TEM) and cross sectional TEM showed the deposited Supermalloy to have a random polycrystalline microstructure with grains of size $\sim$10 nm and a surface roughness of less than 0.5 nm. Scanning electron microscopy (SEM) was used to check the size and shape of the nanomagnets. Figure 1 shows some of these SEM images.

In addition to this structural characterization, we also performed magnetic characterization. Magneto-optical magnetometry was used to measure the coercivity ($\sim$1 Oe) and the anisotropy field (4 $\pm$ 1 Oe, uniaxial in-plane) of the unpatterned film. A B–H looper was used to check its thickness and saturation magnetization (800 $\pm$ 60 emu cm^{-3}). Temperature dependent measurements showed the unpatterned films were still ferromagnetic at 300 °C, which is not inconsistent with the expected Curie temperature of 400 °C and hence an exchange stiffness of $\sim 10^{-6}$ erg cm^{-1} [20].

2.2. Nanomagnetometry

We have probed the room-temperature magnetic properties of the arrays of nanomagnets using a high-sensitivity magneto-optical magnetometer [21], shown schematically in figure 2. The sample surface can be viewed under an optical microscope, while a laser spot (diameter 5 μm) is moved over the surface until it is focused on top of one of the arrays of nanomagnets. The reflected laser beam is then polarization analysed in order to access the longitudinal Kerr effect [22], which serves as a probe of the component of magnetization lying in the optical plane of incidence. An electromagnet allows magnetic fields of up to 1000 Oe to be applied in the plane of the sample. It is necessary to measure *arrays* of nanomagnets in order to obtain a sufficiently large signal. The high definition of the lithography means, however, that all of the particles in the array are virtually identical to each other and so the measured average properties for the array can also be interpreted as the individual properties of a single nanomagnet.

Two different magnetic measurements were made using the magnetometer. The first involved sweeping a field applied in the plane of the sample at 27 Hz and measuring the magneto-optical response. This allowed a hysteresis loop (normalized in amplitude to ± 1) of the nanomagnets to be recorded. The second measurement uses a newly developed technique called modulated field magneto-optical anisometry (MFMA) [23, 24] to probe the energy surface experienced by the magnetization as a function of the in-plane direction. In this technique, a large and static magnetic field, H, is applied in the sample plane *perpendicularly* to the direction of magneto-optical sensitivity. A small transverse oscillating field, H_t, is then applied in the direction of the magneto-optical sensitivity, in order to cause the magnetization to oscillate about H. The measured response (referred to as the transverse susceptibility, once normalized to H_t) can be written as

$$\frac{\partial \phi}{\partial H_t} \equiv \chi_t = \left(\frac{E''(\phi)}{M_s} + H \right)^{-1} \tag{1}$$

where ϕ is the mean magnetization direction, $E''(\phi)$ is the second derivative with respect to ϕ of the energy density surface and M_s is the saturation magnetization. $E''(\phi)/M_s$ is shown in the appendix to have the same magnitude and symmetry as the anisotropy field. Put simply, the reciprocal of the measured magneto-optical response, $1/\chi_t$, is the total internal field in the direction of the magnetization, i.e. the externally applied field H plus the effective anisotropy field coming from the internal energy surface. A powerful probe of the energy surface of the nanomagnet can thus be obtained simply by measuring $1/\chi_t$ as a function of direction and H.

2.3. Micromagnetic modelling

We have used the semi-classical formalism of micromagnetics [3] in order to provide a theoretical framework in which to interpret the experimental data. Micromagnetics is a continuum theory for which a numerical finite-element method is used to find a magnetization vector field which minimizes a Hamiltonian incorporating three energy terms: magnetostatic energy, exchange energy and Zeeman energy. Magnetostatic energy arises from the stray magnetic fields which emanate from any divergence in the magnetization. Magnetization divergence can arise inside a nanomagnet where the magnetization field changes direction ('volume charges') or at the interfaces of the structure where the magnetization is not parallel to the interface ('surface charges'). The high energetic cost of the magnetostatic surface charges means that magnetostatic energy can often be reduced by introducing non-uniformity into the magnetization field. In the lesser cases, this may be a little bending of the magnetization close to the edges of a structure. In more dramatic cases, this may result in the formation of a superstructure within the magnetization field, such as a vortex. These so-called incoherent magnetization fields can reduce the net moment carried by the nanomagnet to zero and so are technologically very important. The calculation of magnetostatic energy is entirely classical. Exchange energy is, in contrast, a quantum mechanical phenomenon and is ultimately responsible for ferromagnetism. A positive exchange energy term arises wherever

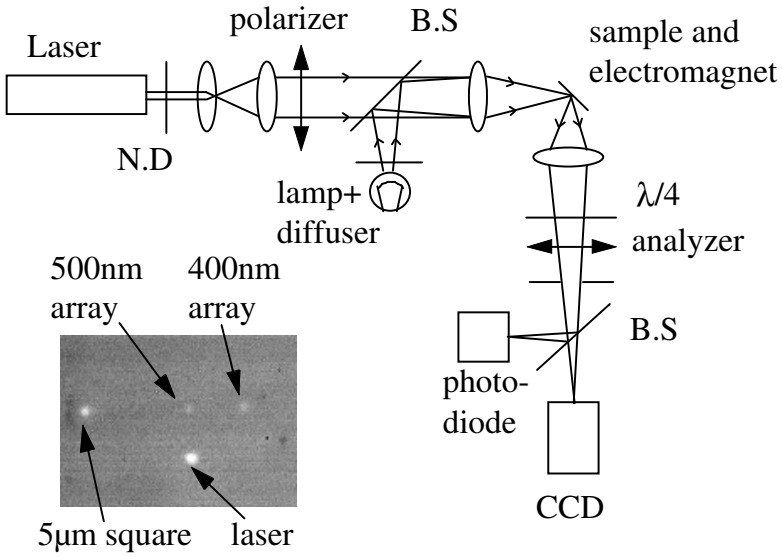

Figure 2. A schematic of the magneto-optical magnetometer used for probing the magnetic properties of nanostructures. Inset is an image recorded by the charge-coupled device camera showing the focused laser spot, an isolated 5 μm square magnet and two 5 μm $\times$ 5 μm arrays of sub-micrometre nanomagnets. B.S denotes the beam splitter and N.D denotes the neutral density filter.

there is a gradient in the magnetization field within a nanostructure. Consequently, exchange energy drives nanostructures away from incoherent magnetization towards uniform magnetization and, is in this sense, in competition with the magnetostatic energy term. The balance point in the competition is ultimately determined by the size, shape and thickness of the nanostructure: large structures are dominated by magnetostatics and small structures are dominated by exchange. The final energy term is Zeeman energy which is simply the energy of the magnetization in an externally applied magnetic field. Zeeman energy is always minimized when the magnetization is aligned with the applied field. A magnetocrystalline anisotropy term would usually also be included in such calculations. We have ignored it for the calculations shown in this paper because it is one to two orders of magnitude smaller in Supermalloy than the other terms.

Figure 3 shows examples of equilibrium magnetization vector fields calculated for square nanostructures. Figure 3(a) shows the vector field (also called a configuration) which occurs when one magnetizes the structure parallel to one of its edges. This configuration is usually poetically named the 'flower' because of the way it flares out at the top and bottom, like the centre of a daffodil. Figure 3(b) shows the configuration associated with a square magnetized along its diagonal. We name this configuration the 'leaf' because of the way that it bows out in the centre and then nips together at the ends, like a plant leaf. We shall discuss the physics of these and other configurations in more detail in section 3.2.

The numerical calculation of an equilibrium magnetization field can be repeated for each value of a varying applied field in order to simulate a hysteresis loop, or as a function of nanomagnet orientation in order to predict anisotropy values. Full details of the numerical algorithm used to implement this formalism can be found in [25].

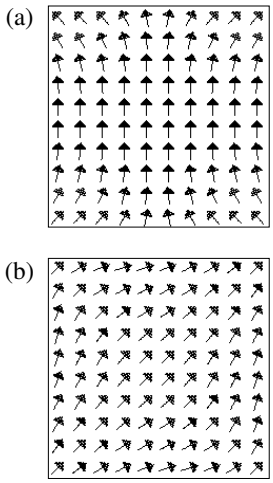

Figure 3. A plan view of the calculated magnetization vector fields in a square nanomagnet of edge length 100 nm and thickness 20 nm when magnetized (a) parallel to an edge and (b) parallel to a diagonal.

3. Results

3.1. Elliptical nanomagnets

3.1.1. Experimental results. Figure 4 shows the hysteresis loops for ellipses of major axis 250 nm, minor axis 125 nm and thickness 10 nm obtained by sweeping an in-plane applied field and recording the magneto-optical signal. One sees clearly that the loop which was measured with the applied field directed along the *major* axis ($\pm 4^\circ$) of the nanostructures displays high remanence and high coercivity, as is characteristic of easy-axis behaviour, whereas that taken along the *minor* axis ($\pm 4^\circ$) of the nanostructures displays near-zero remanence and coercivity, as is characteristic of uniaxial hard-axis behaviour. Supermalloy itself is nearly magnetically isotropic, and so this large difference between

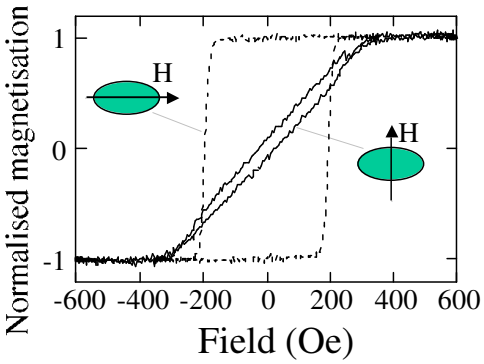

Figure 4. Hysteresis loops measured in two in-plane directions of elliptical nanomagnets of major axis 250 nm and thickness 10 nm.

the major and minor axes must come from magnetostatic shape anisotropy. The hard-axis saturation field (310 ± 15 Oe for the loop in figure 4) is, in such cases, always a good measure of the effective anisotropy field, enabling us to determine the effective uniaxial shape anisotropy field as a function of lateral size and thickness for the ellipses. The results are shown in figure 5 for 1:2 aspect ratio ellipses. For completeness we have also plotted in figure 5 the coercive field as measured from the easy-axis loops. One immediately sees that the uniaxial shape anisotropy and coercivity fall off with increasing ellipse size and increase with increasing thickness. This is usual magnetostatic behaviour, governed by the fact that the demagnetizing field is, to first order, independent of the absolute size of a magnetic element, but depends only on the ratio of the thickness to the lateral size.

3.1.2. Theoretical results. In order to model mathematically the expected shape anisotropy we have used the micromagnetic simulation code described in section 2. This allows the magnetic energy of a nanomagnet to be calculated firstly when magnetized along its major axis and then along its minor axis. The uniaxial shape anisotropy field is then given by $2\Delta U/m$ where ΔU is the difference in these two energies and m is the magnetic moment carried by a nanomagnet. Note that this method takes full account of the deviations from uniform magnetization which occur in a non-ellipsoidal body, such as a planar ellipse. We have used up to 21 870 cubic finite-element cells, each of length 2.5 nm and values of 800 emu cm^{-3} for the saturation magnetization and 1.05×10^{-6} erg cm^{-1} for the exchange stiffness.

We have plotted in figure 6, using a full curve, the results from the micromagnetic calculations for nanostructures of thickness 5 nm alongside the experimental data for this thickness taken from figure 5. One sees that the agreement between the theoretical line and the experimental data is poor: the measured anisotropy fields are in general a factor of two smaller than the theoretical values. This is surprising given that shape anisotropy is a long established concept. In performing the micromagnetic modelling, however, we have assumed the nanomagnets to be perfect ellipses. It is well established that PMMA lithographic processes have a maximum spatial resolution of 5–10 nm [26], due partly to the size and radius of gyration of the PMMA molecules

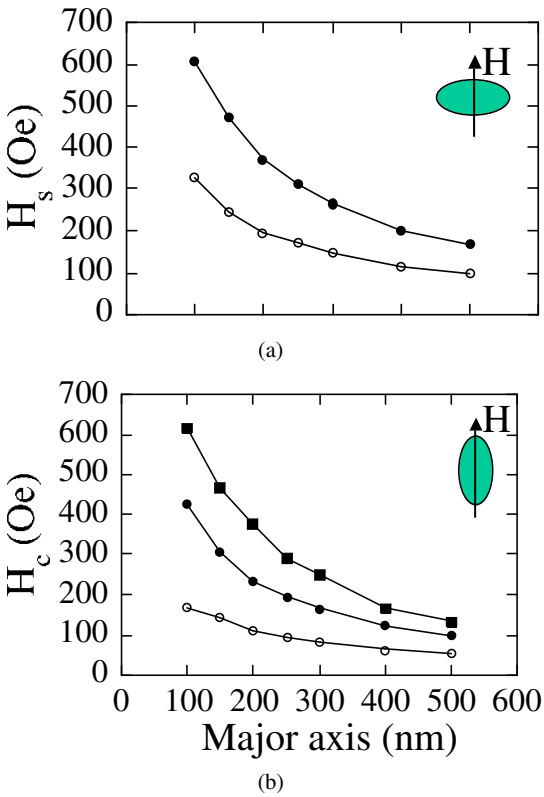

Figure 5. The experimentally measured (a) saturation field in the hard direction and (b) coercive field in the easy direction of elliptical nanomagnets of different size. The nanomagnets were of thickness 5 nm (○), 10 nm (●) and 15 nm (■). The curves are to guide the eye.

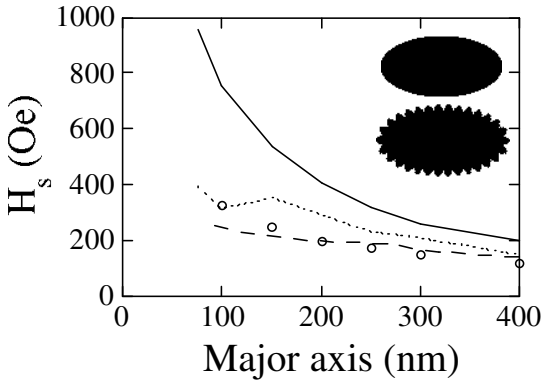

Figure 6. A comparison between experimentally (points) and theoretically (curves) determined shape anisotropy fields for elliptical nanomagnets of thickness 5 nm. The three theoretical lines are calculated assuming an edge roughness of 0 nm (——), 5 nm (· · · · · ·) and 10 nm (- - - -). The insets are 'silhouettes' of two of the modelled ellipses using the same meshing density as used in the calculations, with an edge roughness of 0 nm (upper) and 10 nm (lower).

[27]. Furthermore, the intrinsic grain size of the deposited Supermalloy (∼10 nm) may also limit the lithographic edge definition. The edge definition of the experimental ellipses can thus be no better than approximately 10 nm. We have therefore repeated the modelling, only this time assuming a sinusoidal edge profile of peak-to-peak amplitude ξ (nm)

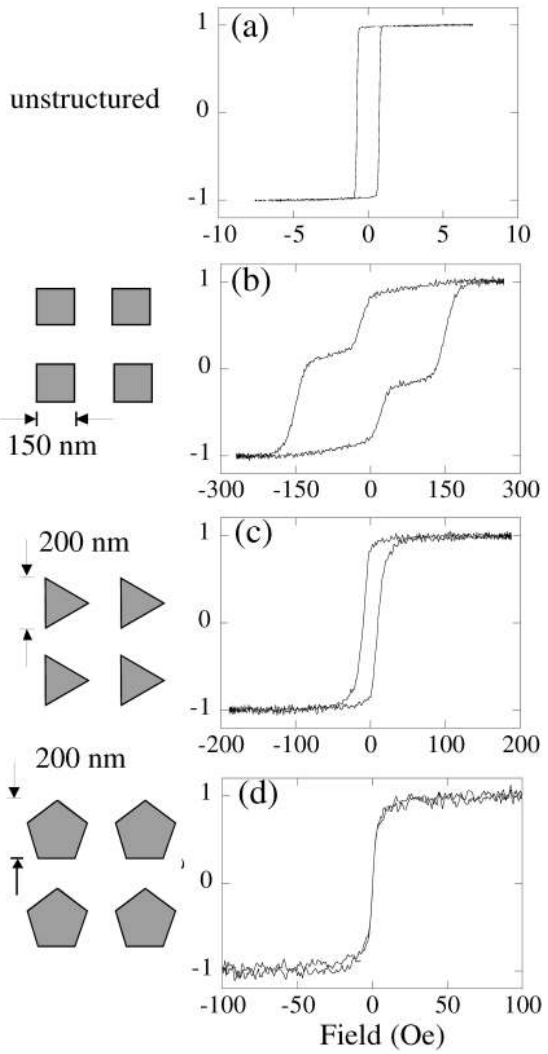

Figure 7. Hysteresis loops measured from different nanostructures. For comparison (a) shows the loop from the unstructured Supermalloy. The y-axis of each graph is magnetization, normalized to the saturation value. The applied field in the schematic pictures of the nanostructures is assumed to point up the page. The nanostructures had thicknesses of (a) 6 nm, (b) 5 nm, (c) 5 nm and (d) 3 nm.

and wavelength 2ξ (nm). Figure 6 shows the result of this calculation (assuming again a thickness of 5 nm) for two different values of ξ. The insets in figure 6 are 'silhouettes' of two of the modelled ellipses using the same meshing density as used in the calculations. The agreement between experiment is now much improved. The edge roughness clearly plays a vital role; the effective shape anisotropy of the ellipses, even as large as 500 nm, can be reduced by a factor of just under two simply by introducing a few nanometres of roughness to the lateral interfaces. Figure 6 shows the best agreement between the experiment and theory for an edge roughness of between 5 and 10 nm, which is entirely consistent with the PMMA grain size. This is also consistent with recent numerical results from Gadbois *et al* [28] who found a significant reduction in the switching fields of elongated magnetic memory elements once a small edge roughness was introduced into the calculations.

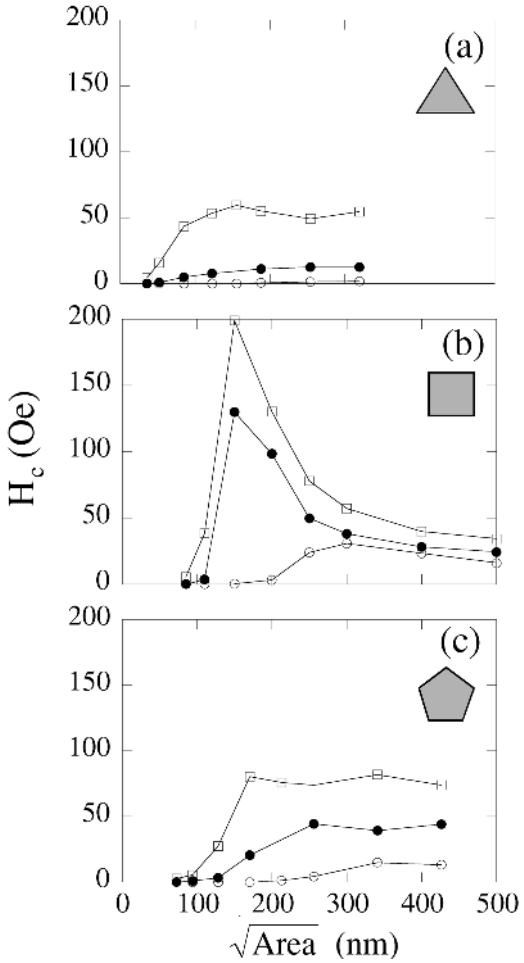

Figure 8. Experimentally measured coercivities as a function of nanomagnet size for different thicknesses (3 nm (○); 5 nm (●) and 7.5 nm (□)) and nanomagnet geometries: (a) triangle, (b) square and (c) pentagon.

3.2. Triangular, square and pentagonal nanomagnets

Figure 7 shows a selection of some of the hysteresis loops measured from nanomagnets of triangular, square and pentagonal shape [29]. One immediately sees that the loops are very different from each other and from that obtained from the conventional unstructured material. The properties covered range from those usually associated with moderately 'hard' magnetic materials with switching fields of hundreds of oersteds (Figure 7(b)) down to those associated with very 'soft' magnetic materials with a high relative permeability suitable for field sensing (e.g. the pentagons of figure 7(d) with an effective relative permeability of 3000 and zero hysteresis). These changes in properties are a direct result of varying the thickness and, most importantly, the symmetry of the nanomagnets in the arrays.

In order to quantify the effects of shape, size and thickness more precisely, we have measured the three key magnetic parameters, coercivity, susceptibility ($4\pi M_s$ times the zero-field gradient of the normalized hysteresis loop), and hysteresis ($4\pi M_s$ times the area of the normalized hysteresis loop), from the loops as a function of size, thickness and symmetry order of the nanomagnets. The results are shown

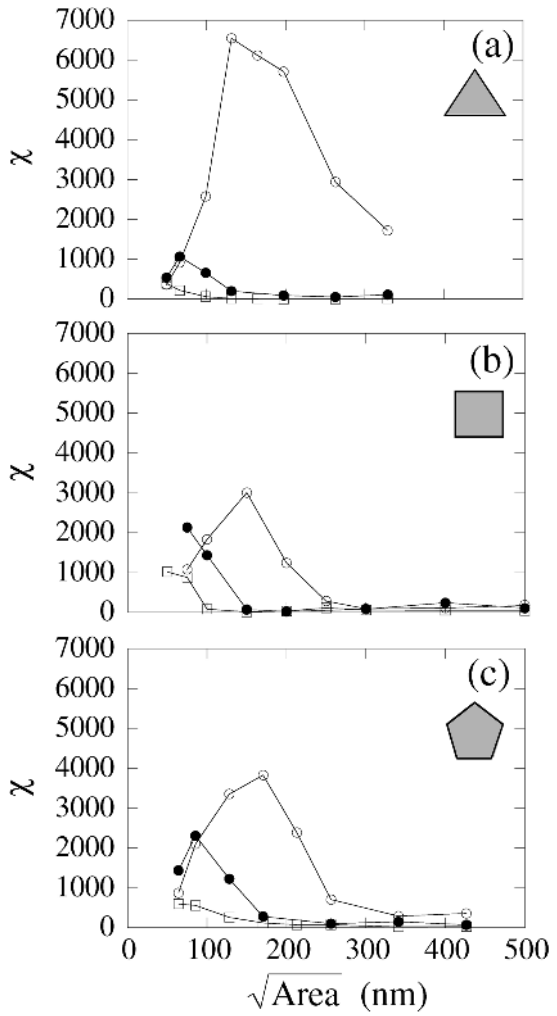

Figure 9. Experimentally measured susceptibilities as a function of nanomagnet size for different thicknesses (3 nm (○); 5 nm (●) and 7.5 nm (□)) and nanomagnet geometries, see figure 8.

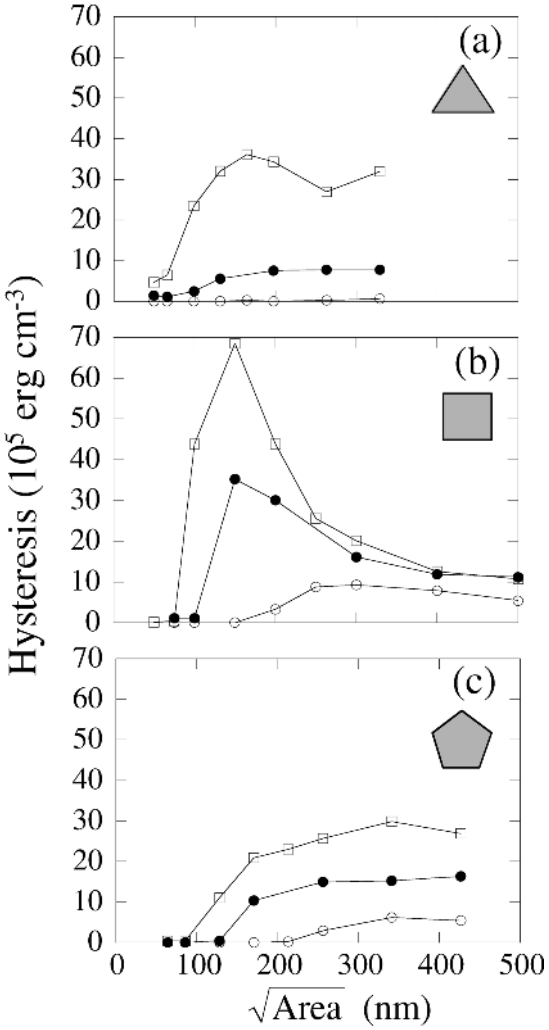

Figure 10. Experimentally measured hysteresis as a function of nanomagnet size for different thicknesses (3 nm (○); 5 nm (●) and 7.5 nm (□)) and nanomagnet geometries, see figure 8.

in figures 8–10, where, in order to be able to compare different geometries, we express the size of the nanomagnets by the square root of their area.

Despite the large volume of experimental data presented across these three figures, one can see certain common features. The coercivity (figure 8) and hysteresis (figure 10) data both show a rise or plateau as the nanomagnet size is reduced, followed by a sharp fall to zero. As the thickness is increased, both coercivity and hysteresis increase and the fall to zero coercivity and hysteresis occurs at smaller sizes. The squares show much stronger peaks in these two data sets than the triangles and pentagons.

The susceptibility data (figure 9) tracks the coercivity and hysteresis data, but in the opposite sense. One sees that as the size decreases, susceptibility at first remains constant or falls slightly, but then rises sharply. The thinner nanomagnets then show an additional fall in susceptibility as the size is further decreased. As the thickness is increased, susceptibility is reduced and the susceptibility peak occurs at smaller sizes.

Coercivity, hysteresis and susceptibility are all determined by anisotropy. The fact that one sees such strong variations in these three parameters as the size and thickness vary, and hence a strong change in the shape of the hysteresis loops of figure 7, suggests that the nanomagnets possess a size-dependent anisotropy. We have therefore used the magneto-optical magnetometer in MFMA mode to measure directly the magnitude and symmetry of any anisotropy in the nanomagnets of thickness of 5 nm, and we present the results in figure 11. In these polar plots, the angle gives the in-plane direction ϕ within the nanomagnet, the radius gives the radius of the nanomagnet in that direction and the colour gives the experimentally measured quantity $\partial H_t/\partial\phi$ (and hence the anisotropy field—see equation (1)) for a nanomagnet of that size. Figure 11 shows experimental data from 22 different arrays of nanomagnets (eight sizes of triangles, eight sizes of squares and six sizes of pentagons), each measured in either 19 or 37 different directions ϕ (0–180° in 10° steps for triangles and squares and 0–180° in 5° steps for pentagons) making a total of 526 experimental measurements.

It is readily apparent from figure 11 that there are indeed strong anisotropy fields present in all of the nanomagnets studied. The triangular nanomagnets exhibit anisotropy with 6-fold symmetry, the square nanomagnets show a 4-fold

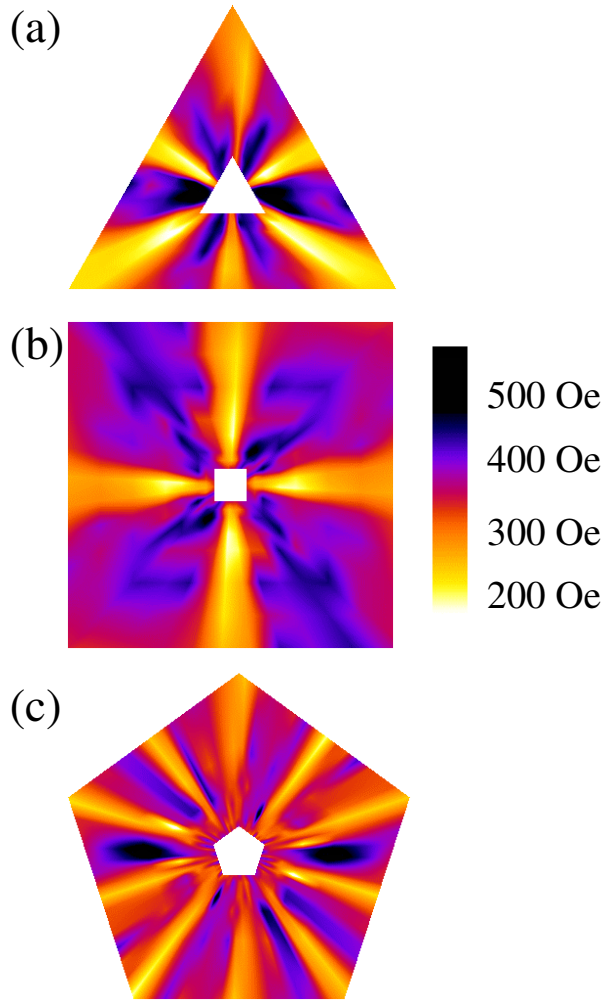

Figure 11. The experimentally measured anisotropy field inside 5 nm thick nanomagnets of (a) triangular, (b) square and (c) pentagonal symmetry. These are colour polar plots where the direction gives the in-plane direction in the nanomagnet, the radius gives the nanomagnet radius in that direction and the colour gives the experimentally measured anisotropy field of a nanomagnet of that size. High field values correspond to easy anisotropy axes and low values to hard anisotropy axes. The lateral scale of the figure is such that the square data runs from edge length 50 nm to 500 nm. Data were recorded across a 180° range and then plotted twice to fill 360°.

symmetric anisotropy and the pentagonal nanomagnets possess a remarkable 10-fold anisotropy. Frequency doubling occurs in the triangular and pentagonal structures because energy is always quadratic in the magnetization and so odd symmetry orders cannot be supported.

We applied a Fourier analysis to the plots of figure 11 in order to obtain the magnitude of the anisotropy fields as a function of the nanomagnet size and symmetry, and show the results in two different forms in figure 12. The appendix shows that the anisotropy energy U and the anisotropy field H_a of any system are related by

$$U = \frac{2M_s V H_a}{n^2} \qquad (2)$$

where n is the symmetry order of the anisotropy and V is the volume of the particle (a single nanomagnet in this

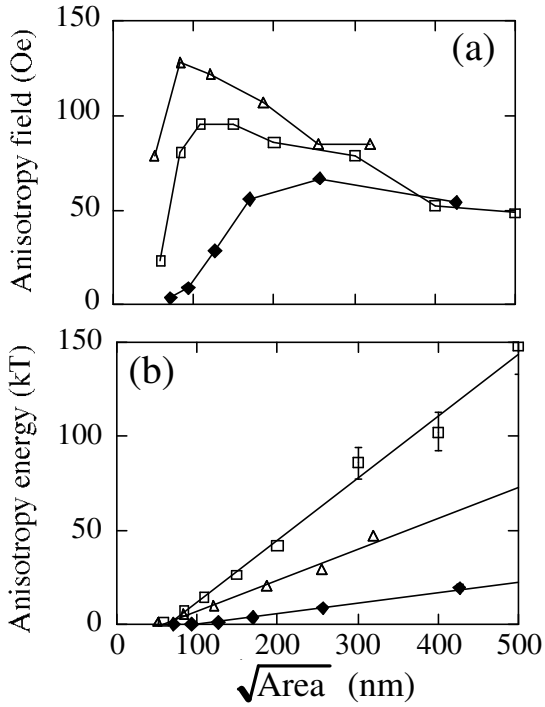

Figure 12. The strength of the dominant anisotropy term shown in figure 11 expressed (a) as an anisotropy field and (b) as an anisotropy energy per nanomagnet for nanomagnets of different size and symmetry (triangles (△), squares (□) and pentagons (⧫)).

Table 1. Experimentally determined values for the parameters C and l_0 of equation (3).

Shape	n	C (nm^{-1})	l_0 (nm)	Cn^2 (nm^{-1})
Square	4	0.33 ± 0.03	59 ± 6	5.3 ± 0.5
Triangle	6	0.16 ± 0.02	55 ± 3	5.9 ± 0.7
Pentagon	10	0.05 ± 0.005	79 ± 20	5.0 ± 0.5

case). In figure 12(a) we plot the anisotropy *fields* directly, as returned by the MFMA experiment, whereas in figure 12(b) we have plotted the anisotropy *energy* of a single nanomagnet (in units of kT where k is the Boltzmann constant and T is 298 K) using equation (2). Importantly, one sees in this figure that whereas the anisotropy *fields* show an initial rise with increasing lateral size, which then either falls again (squares and triangles) or forms a plateau (pentagons), the anisotropy *energy* can be described approximately by the straight line relationship

$$\frac{U}{kT} = C(\sqrt{Area} - l_0) \qquad \text{when } U > 0 \qquad (3)$$

where the experimentally determined parameters C and l_0 are given in table 1. The table also shows that the quantity Cn^2 is found to be approximately constant across all nanostructures (at one thickness). This thus gives us a useful phenomenological tool for rapidly assessing how magnetic properties are influenced by size and symmetry.

The anisotropy energy is particularly interesting because of a phenomenon called superparamagnetism [30], which is the process by which anisotropy energy barriers can be overcome by the kT thermal energy fluctuations in nanometre

scale magnets. One would thus expect the coercivity and hysteresis to fall to zero once the anisotropy energy becomes comparable to a few kT (the precise prefactor depends upon the symmetry order of the anisotropy and the timescale over which the experimental measurements are made). The phase transition from ferromagnetism to superparamagnetism should also be accompanied by a peak in the susceptibility at the critical point of the phase transition. Conversely, once the anisotropy energy is larger than a few kT, the coercivity and hysteresis should approximately follow the anisotropy field and the susceptibility should be low. This is all consistent with the observations of figures 8–10 for 5 nm thick structures. The anisotropy field of the squares shows a peak in figure 12(a) as the element size is reduced and this peak is reflected directly in the square coercivity data (figure 8) and the hysteresis data (figure 10). The pentagon anisotropy field shows no peak, and this is also reflected directly in the coercivity and hysteresis data. Finally, the triangle anisotropy field does show a peak just like the square, but because the anisotropy *energies* are lower in the triangle (due to the high value of n in equation (2)), thermal activation sets in at a larger size and prevents the peak from being seen in the coercivity and hysteresis data. The anisotropy energies (figure 12(b)) fall below a few kT at around 80 nm and this is approximately where one sees a peak, or one side of a peak, in the 5 nm thick susceptibility data (figure 9). It is interesting to note that the susceptibility peak occurs at much larger lateral sizes and has a much greater amplitude in the 3 nm thick structures. This is because the configurational anisotropy field is reduced because of the dependence of the demagnetizing field on the ratio of the thickness to the lateral size. This reduced configurational anisotropy field then becomes an even more reduced anisotropy energy because of the V term in equation (2). Superparamagnetism in very thin structures therefore begins at much larger lateral sizes. The high magnetic softness which results could have important applications in magnetic sensors.

An important question remains: why should the geometric shapes studied in this section exhibit any anisotropy at all? The demagnetizing field of any structure is described by a second rank Cartesian tensor and so can only exhibit uniaxial (2-fold) symmetry. There is therefore *no shape anisotropy* present, at least in the conventional sense, in the plane of these non-elongated higher-order symmetry structures. The answer comes from a phenomenon called *configurational anisotropy*. First proposed by Schabes and Bertram [31] during a theoretical study of magnetic cubes, we recently predicted [32] and observed experimentally [23] its key role in planar magnetic nanostructures, such as those described in this paper. The demagnetizing field is only uniform in an ellipsoidal body and so must be non-uniform in any finite planar structure. This can be seen in the micromagnetic simulations of planar squares shown in figure 3. The important point to realise is that the two configurations shown in figure 3 *have different energies*. This is entirely due to the deviations from uniform magnetization which they exhibit. Consequently, although the energy of a perfectly uniformly magnetized square is independent of the in-plane magnetization direction, as soon as one takes into account the non-uniformity of the magnetization which must accompany a given magnetization direction, energy differences do arise. An anisotropy thus appears with a symmetry which is related to that of the geometric shape of the nanostructure. This is called configurational anisotropy because it comes from the differences in energy of the different configurations (flower and leaf in the case of a square) which arise as the magnetization direction is varied.

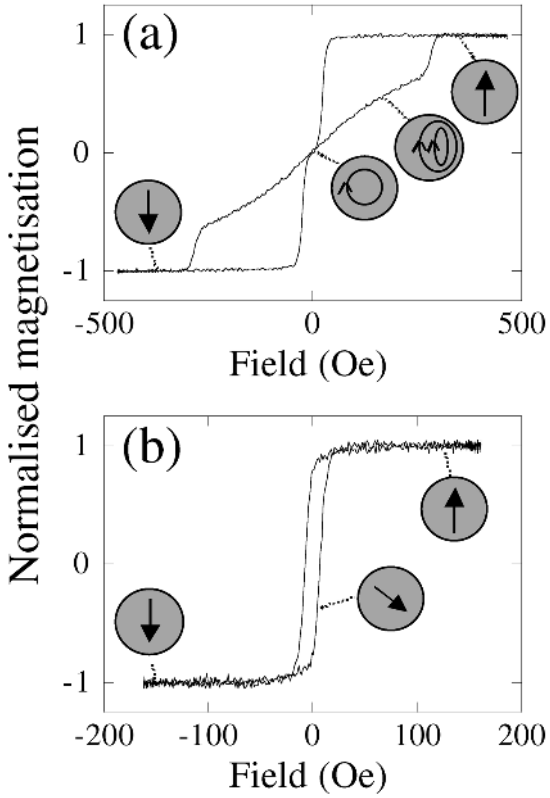

Figure 13. Hysteresis loops measured from circular nanomagnets of diameter (d) and thickness (t): (a) $d = 300$ nm, $t = 10$ nm and (b) $d = 100$ nm, $t = 10$ nm. The schematic annotation shows the magnetization within a circular nanomagnet, assuming a field oriented up the page.

3.3. Circular nanomagnets

Circular nanomagnets are potentially very attractive for many technological applications. Their circular form means that they lack both shape anisotropy and configurational anisotropy. If they are made from an intrinsically isotropic material, it should therefore be possible to change their magnetization direction by even very weak applied magnetic fields. They could thus form the heart of an extremely sensitive magnetic field sensor. More fundamentally, one of the most important theorems in nanomagnetism is Brown's fundamental theorem [33] which states that, because of a competition between magnetostatic energy and quantum mechanical exchange energy, magnetic domain formation should be entirely suppressed in very small ($\sim 10^{-8}$ m) magnetic particles, causing nanomagnets to behave as single giant spins. Experimental data on the bounds of validity of Brown's theorem in well controlled systems are currently in great demand.

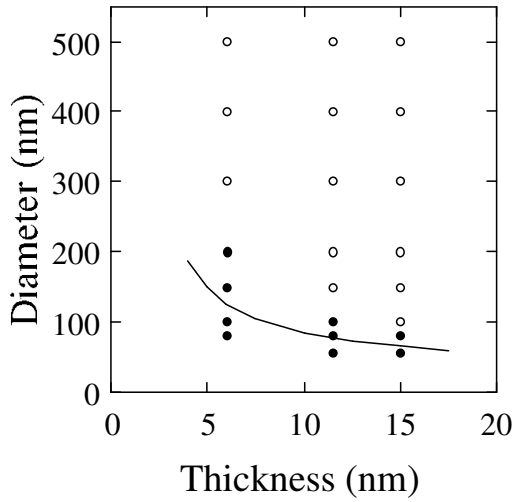

Figure 14. An experimentally determined phase diagram: vortex (○) and single domain (●). The solid line shows a lower bound to the theoretical phase boundary between the vortex state (above the boundary) and the single domain state (below the boundary).

3.3.1. Experimental results. We have measured hysteresis loops from circular nanomagnets as a function of diameter (50–500 nm) and thickness (6–15 nm) [34]. We find that the hysteresis loops thus obtained fall into one of two classes. Figure 13 shows a representative hysteresis loop from both of these classes with schematic annotation. The first class, which we call the 'vortex phase' is typified by the 300 nm/10 nm loop (figure 13(a)) as follows. As the applied field is reduced from minus saturation, the nanomagnets retain full moment, until a critical field slightly below zero at which point nearly all magnetization is lost. The magnetization then progressively reappears as the field is increased from zero, until positive saturation is achieved. The sudden loss of magnetization close to zero field is very characteristic of the formation of a flux closing configuration; the simplest of these is a vortex in which the magnetization vector remains parallel to the nearest edge at all points in the circular nanomagnet. In large structures, this state lowers the system energy by reducing stray fields and hence lowering magnetostatic energy. Increasing the field then deforms the vortex by pushing its core away from the centre of the nanomagnet, until it becomes unstable and the vortex is eventually annihilated [35], although not until a field of several hundred oersted has been reached. This vortex phase leads to magnetic properties which are dramatically different from those which would occur if the magnetization simply rotated under the action of a weak field.

The second class of loop, which we call the single domain phase, is typified by the 100 nm/10 nm loop (figure 13(b)). These loops retain a high remanence ($\sim 80\%$) and switch at a very low field (~ 5 Oe). This is characteristic of single domain behaviour: all of the nanomagnets within the array retain all of their magnetization to form an array of giant spins, and magnetization reversal occurs by each giant spin rotating coherently [36]. The absence of shape anisotropy (except that due to any ellipticity in the nominally circular shape) and configurational anisotropy then means that the only anisotropy opposing the coherent rotation is the weak in-plane anisotropy intrinsic to the Permalloy family. Hysteresis loops of this class thus have a saturation field of merely a few oersted. We found that the remanence vanished if the field was applied parallel to the uniaxial hard axis instead of the easy axis, as would be expected for such a reversal mechanism.

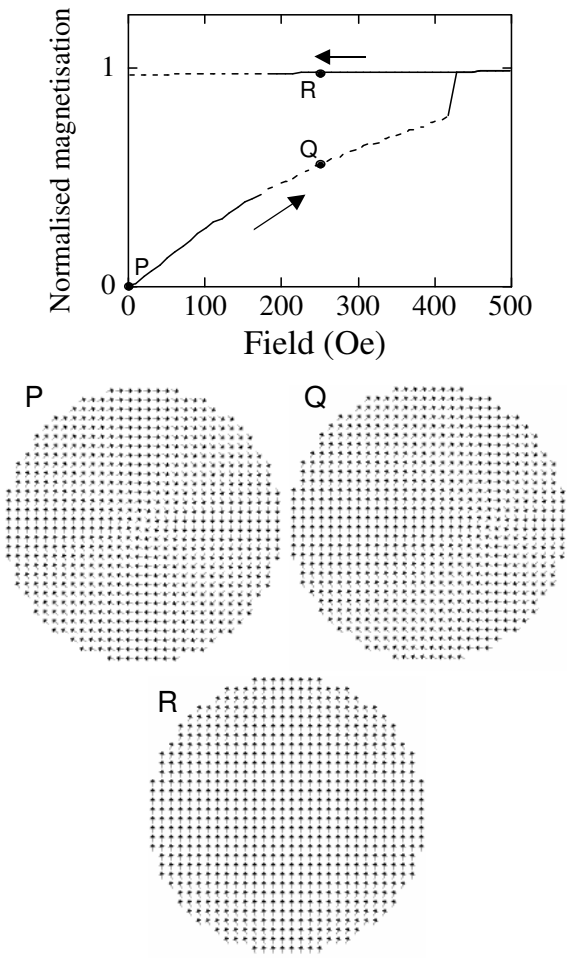

Figure 15. A theoretically determined hysteresis half loop for a circular nanomagnet of diameter 300 nm and thickness 10 nm (and so should be compared with figure 13(a)). The broken curve parts of the loop indicate a metastable state. The calculated magnetization vector fields are shown for three points on the loop P, Q and R, assuming a field oriented up the page.

We have classified all of our experimental data from circular nanomagnets in terms of vortex or single domain behaviour and have plotted the result in figure 14.

3.3.2. Theoretical results. In order to verify that the class of behaviour typified by figure 13(a) is indeed due to vortex formation we performed micromagnetic calculations to simulate one half of the loop, in which 5656 cubic finite-element cells, each of length 5 nm, were used.

Figure 15 shows the half-loop which we have calculated for a circular nanomagnet of diameter 300 nm and thickness 10 nm (i.e. the same size as that measured in figure 13(a)). The precise mechanism by which a vortex is first nucleated is highly complex and is beyond the scope of this study. We therefore assume that a vortex is present under zero field.

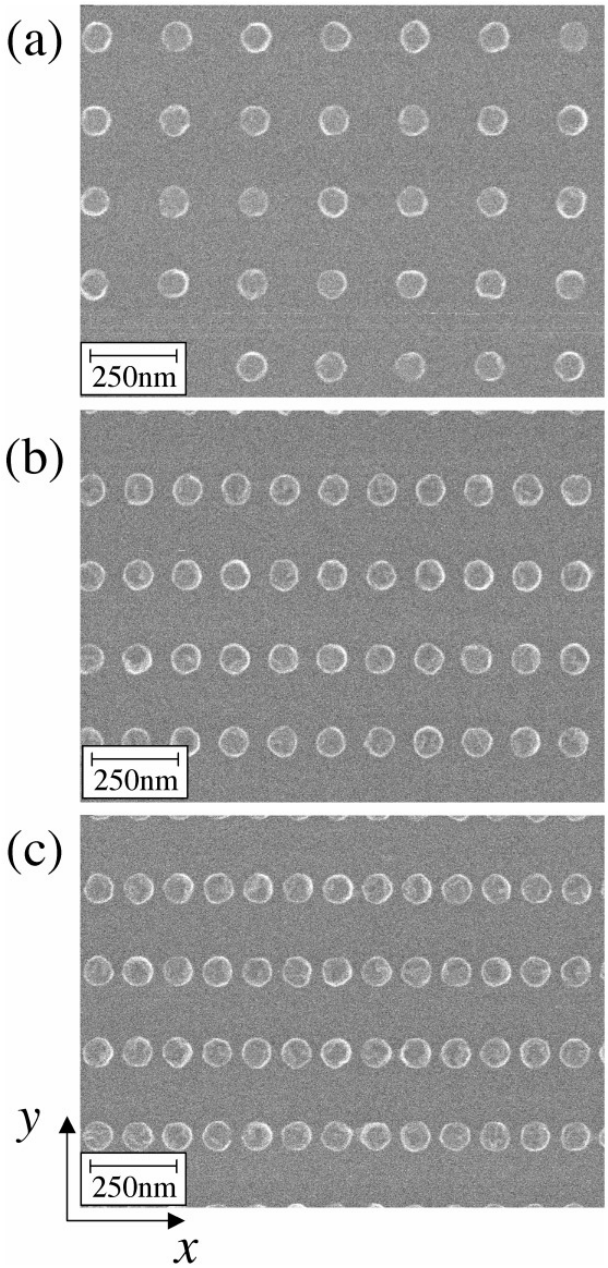

Figure 16. SEM images of rectangular lattices of circular nanomagnets. Each nanomagnet is 60 nm in diameter and has a y-direction lattice parameter of 180 nm. The x-direction lattice parameter is (a) 180 nm, (b) 110 nm and (c) 90 nm.

One sees that as the applied field is increased from that point, the calculated loop traces out an almost identical path to that obtained experimentally in figure 13(a). Both show a small degree of curvature followed by an abrupt annihilation event at a field of several hundred oersted. Figure 15 also shows the calculated magnetization vector fields within a single circular nanomagnet at three different points on the hysteresis loop. These agree well with the schematic representations shown in figure 13(a).

We have marked parts of the theoretical half-loop of figure 15 by a broken curve. These correspond to metastable regions, i.e. those for which the magnetization configuration leads to a local minimum in the free energy, but not a global

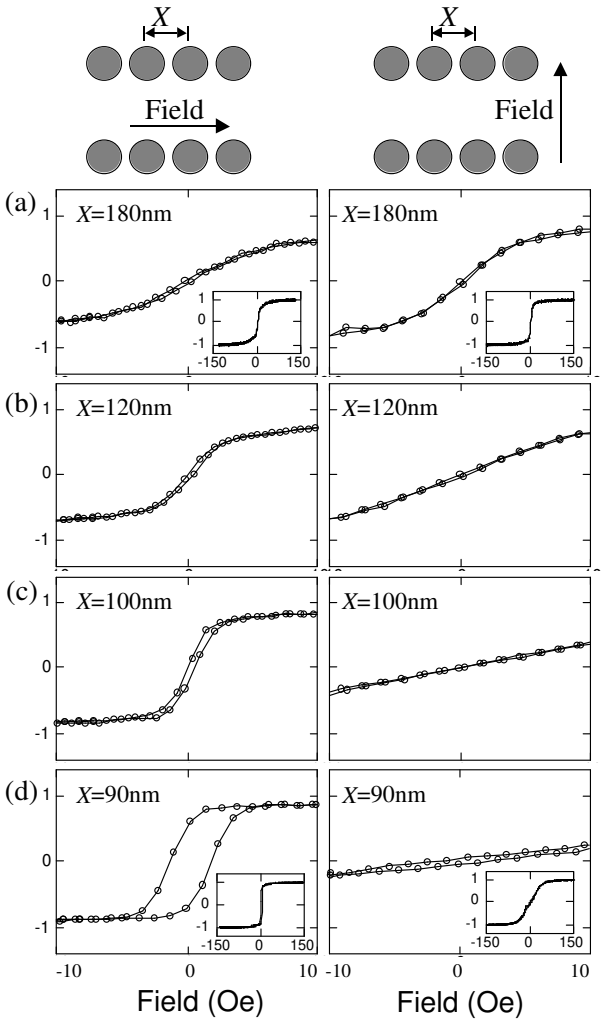

Figure 17. Experimentally measured hysteresis loops for different lattice spacings and applied field directions. All loops were measured within the field range ±150 Oe, the large panels show high-magnification views around zero field; the insets show the full measured loop. The vertical axis of all loops is magnetization normalized by the saturation value.

minimum. Whether a thermally activated transition from the metastable state to the thermodynamic ground state is to occur depends upon the temperature and the timescale over which the hysteresis loop is swept out. The theoretical simulation of figure 15 does not allow for thermally activated transitions, which accounts for the difference between the experimental and theoretical vortex annihilation fields of 283 Oe and 423 Oe respectively.

As the lateral size and thickness of the nanomagnets is decreased, our calculations show that the range of applied fields for which the vortex state is metastable increases until the vortex can never nucleate and so the reversal mechanism must be replaced by the Stoner–Wohlfarth coherent rotation shown in figure 13(b). We have marked onto the experimental phase diagram of figure 14 the calculated phase boundary below which vortex nucleation is impossible. One sees that the experimental data agree very well with the theoretical line: no vortex nucleation was observed below it. We stress that the theoretical line is *not* a prediction for the transition

from vortex to single domain behaviour, but is rather a lower limit to that boundary. Experiment and theory are thus in agreement: in order to observe the useful single domain state, circular nanomagnets must be either very thin or laterally small.

3.4. Interacting nanomagnets

So far in this section we have discussed the influence of the shape of nanomagnets on their magnetic properties. All of the experiments performed in our study and many of the potential technological applications of nanomagnets do not use a single nanomagnet, but rather a large ensemble of magnets arranged on some lattice. If the lattice spacing is sufficiently small (expressly not the case in the work described so far), the magnetic field emanating from one nanomagnet can influence its neighbours. In this case, one must also consider the geometry of the *lattice* as well as the shape of the motif.

In order to demonstrate and investigate the phenomenon of magnetostatic interactions, we have made a number of arrays of 60 nm diameter circular nanomagnets arranged on a rectangular lattice [37]. The y-direction lattice period was kept constant at 180 nm (i.e. three times the diameter of the nanomagnets) whereas the x-direction lattice period varied in different arrays from 180 nm down to as small as 80 nm (i.e. leaving only 20 nm between neighbouring edges). Figure 16 shows SEM images of some of the lattices.

Figure 17 shows hysteresis loops obtained from the different lattices for the cases of the field applied along the lattice x- and y-directions. One sees that when the nanomagnets are widely separated (e.g. figure 17(a)) the hysteresis loops have a characteristic 'S' shape, are fully closed (i.e. zero area inside the loop) and are virtually identical in the two measurement directions. As the x-axis spacing is reduced, however, the loops show a significant change in their central region, the x-axis loop opening up while the y-axis loop becomes more sheared (e.g. figures 17(c) and 17(d)).

Each nanomagnet, being 60 nm in diameter and 7 nm thick, is small enough to be in the single domain state (cf figure 14) and can therefore be represented, to a good approximation, as a point magnetic dipole located at the nanomagnet centre. The magnetic field emanating from such a magnetic dipole falls off with the cube of the distance from it. The largest lattice period ($X = 180$ nm—see figures 16(a) and 17(a)) causes the nanomagnets to be spaced by three times their own diameter, which is a sufficiently large distance for magnetostatic interactions between nanomagnets to be relatively weak. The measured average property of the lattice is, thus, approximately the same as the individual property of an isolated nanomagnet, as in all of the other experiments reported so far in this paper. In this case, the weak intrinsic uniaxial anisotropy of Supermalloy is unable to stabilize the zero-field magnetization against thermal fluctuations (in contrast to the larger single domain particles measured in figure 13(c)), leading to a time-averaged remanence of zero, and hence the closed, superparamagnetic hysteresis loops of figure 17(a).

As the separation between the nanomagnets is now reduced, as shown in figures 16(b) and 16(c), the magnetostatic coupling between nanomagnets (especially, but not exclusively, between nearest neighbours) becomes stronger, to the point at which it can overcome the thermal fluctuations. When this occurs, the spins essentially remain parallel and locked together in the x-direction even under zero applied field, leading to increased remanence in the x-direction loops of figures 17(c) and 17(d).

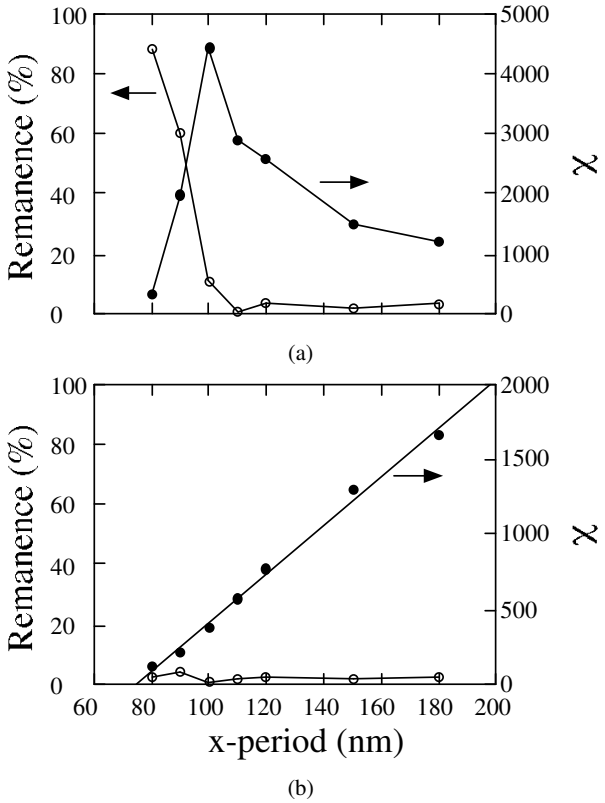

Figure 18. Remanence (open circles) and susceptibility (full circles) measured as a function of lattice spacing for the field applied along (a) the lattice x-direction and (b) the lattice y-direction.

Magnetostatic coupling is an anisotropic coupling, with an energy minimum (easy axis) when the dipoles are aligned with the line joining their centres (i.e. the x-direction in this experiment) and an energy maximum (hard axis) when aligned perpendicular to this line (i.e. the y-direction). Consequently, whereas the remanence rises in the loops measured in the x-direction, the loops measured in the y-direction become increasingly sheared as a uniaxial hard direction appears.

We showed earlier in this paper how the shape of a nanomagnet can induce configurational anisotropy which can overcome thermal fluctuations and thus lead to abrupt changes in the susceptibility, remanence and coercivity. In the case of interacting particles, the anisotropy induced by the rectangular lattice can give the same effect. Figure 18 shows the susceptibility (labelled χ_T this time) and remanence measured experimentally in the lattice x- and y-directions as a function of the lattice x-direction spacing. One sees in Figure 18(a) a peak in the susceptibility at $X = 100$ nm coinciding with the onset of remanence, in direct analogy with the peak in susceptibility in figure 9 coinciding with the rise of coercivity (figure 8) and hysteresis (figure 10).

As expected, no peak in susceptibility is observable in the y-direction of the lattice (figure 18(b)) because this is now the 'hard' magnetization direction and so never displays remanence. The effect of magnetostatic interactions is nevertheless still very much in evidence with the susceptibility falling with decreasing separation as the nanomagnets become increasingly coupled. The fact that the x- and y-direction susceptibilities do not become exactly equal in the limit of $X = Y = 180$ nm is due to the presence of weak uniaxial anisotropy in the Supermalloy and other experimental artefacts.

4. Discussion

The experimental and theoretical results presented above have highlighted the two important ways in which a nanomagnet's shape influences its magnetic properties. The first is the extent to which the shape introduces anisotropy. This anisotropy then determines all of the macroscopic magnetic parameters such as coercivity, remanence, hysteresis and susceptibility. Unsurprisingly, elongated shapes such as ellipses and rectangles introduce a uniaxial shape anisotropy. Shape anisotropy is an interaction between the mean magnetization direction and the form of the nanomagnet, i.e. it occurs even in perfectly uniformly magnetized structures, such as ellipsoids. Shape anisotropy is in this sense a phenomenon associated with the zeroth spatial order of the magnetization field. More surprisingly, non-elongated shapes which possess a definite rotational symmetry, such as triangles, squares, pentagons, etc, also introduce an anisotropy related to their size and symmetry, called configurational anisotropy. Configurational anisotropy is an interaction between the deviations of the magnetization from uniformity and the form of the nanomagnet. It is therefore a phenomenon associated with first and higher spatial orders of the magnetization field.

The second way in which a nanomagnet's shape influences its magnetic properties is the extent to which it stabilizes a single domain state, by preventing incoherent magnetization fields such as vortices or domain patterns. Size alone can do this, as was demonstrated in the circular nanomagnets, which were found to be single domain for sizes less than approximately 100 nm. Form can also play an important role: all of the elliptical, triangular, square and pentagonal nanomagnets were found to be single domain, even at sizes as large as 500 nm. There are two reasons for this. The first is associated with the sharp angles between edges in shapes such as triangles. These increase the energy of vortices because of the sharp turn, and hence the increased exchange energy, which occurs if the magnetization is to remain parallel to the edges. The second reason is more applicable to elongated structures and concerns anisotropy. Anisotropy generally encourages the single domain state over vortex formation because, in the former case, the system can lower its energy by aligning all of the magnetization with an anisotropy easy direction. Incoherent magnetization distributions usually have a proportion of the magnetization in the anisotropy hard direction. Thus, although we have presented the influence of shape on magnetic properties as being comprised of two separate issues, i.e. anisotropy and stabilizing the single domain state, the two are actually linked because anisotropy itself stabilizes the single domain state at remanence.

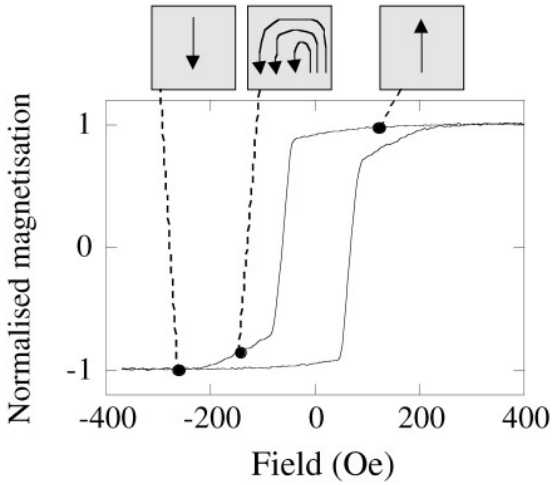

Figure 19. An experimentally measured hysteresis loop from square nanomagnets of edge length 400 nm and thickness 10 nm. The schematic annotation shows the magnetization field assuming the positive applied magnetic field to be pointing up the page.

So far we have discussed the stability of the single domain state at remanence. This, however, is not the only case of interest. Incoherent magnetization structures as a vehicle for achieving magnetization reversal are also important, i.e. a nanomagnet can be single domain under zero field, but then go via a vortex or similar state as the magnetization changes direction under the action of an applied field. We have not discussed the microscopic details of switching mechanisms in this paper except to postulate that the very small circular nanomagnets switch by coherent rotation. The reason for our silence on this subject is that hysteresis loops are not a good tool for investigating the microscopic details of magnetization reversal. Direct imaging, such as Lorentz microscopy [38] or spin-polarized SEM [39] are really required for this. Nevertheless, one can infer a certain amount about the reversal mechanism from hysteresis loops. Figure 19 shows a hysteresis loop measured from 10 nm thick squares of edge length 400 nm. As described earlier, the loop shows almost full remanence, even though a circle of such dimensions would have most certainly collapsed into a vortex at remanence. There is then the usual abrupt coercive transition as the magnetization begins to change direction. This jump does not, however, achieve full switching, but rather leads into a more gentle slope which eventually takes the magnet into saturation. Our explanation for this is that the initial abrupt transition was not to a fully reversed single domain state but to some incoherent distribution such as the 'U' shaped buckle shown in the schematic annotation of figure 19. The gentle slope then follows the further distortion and eventual annihilation of the buckle. Thus, even though geometric shaping had suppressed incoherent magnetization *at remanence*, domains are still involved in the reversal process at higher fields. Defects in the nanomagnets will certainly play some role in the nucleation and annihilation of the buckle structure, although further experiments are required to establish their precise role.

Exchange energy and magnetostatic energy were introduced in section 2 as 'natural enemies': magnetostatic energy is minimized by non-uniform magnetization, exchange energy is minimized by uniform magnetization. The simplest application of this competition principle can be seen in figure 14 where small, circular structures are dominated by exchange energy and so show the single domain state and large circular structures are dominated by magnetostatic energy and so show the vortex state. We can, however, go further than this and say that the exchange-magnetostatic competition is also evident in the phenomenon of configurational anisotropy. As we have already stated, configurational anisotropy is a property of non-uniform magnetization fields. The degree of the non-uniformity and hence the strength of the configurational anisotropy are, however, dictated by the exchange-magnetostatic competition. This can be seen in figure 12(b) where the configurational anisotropy energy is seen to depend upon the nanomagnet's size by a straight line relationship. The straight line does not, however, pass through zero, but rather cuts the x-axis at around 60 nm (l_0 in table 1). This is the size at which exchange begins to dominate the structure and so suppresses non-uniformity in the magnetization field, leading to a collapse in the configurational anisotropy. The l_0 offset, and hence the exchange-magnetostatic competition, can even be shown to be responsible for all of the peaks at around 100–150 nm in the experimental data of figures 8–10 and 12. Suppose that the configurational anisotropy energy varied in a perfectly linear fashion with the square root of the area (i.e. $l_0 = 0$ in equation (3)). Substituting equation (3) into equation (2) would then give

$$H_a = \frac{CkTn^2}{2M_s t\sqrt{A}} \tag{4}$$

where t is the thickness of the nanomagnet, i.e. the configurational anisotropy field would vary with the reciprocal of the nanomagnet size, showing a divergence as that size is reduced to zero instead of the rise and subsequent fall which one sees in figure 12. The high magnetic softness which we have observed in small nanomagnets of definite geometric shape is therefore another example of the dominance of exchange over magnetostatic energy in very small structures, and is in this sense the same phenomenon as that which causes the single domain phase in figure 14.

We concluded section 3 with a description of magnetostatically interacting circular nanomagnets. We showed that the shape of the *lattice* could be imposed on the nanomagnets' properties through magnetostatic interactions. In that case, we showed how uniaxial properties developed. This is analogous to shape anisotropy, i.e. a uniaxial magnetic property arising from a difference in the experimental lengthscales of two orthogonal directions. Just as perfectly uniformly magnetized particles can only exhibit shape-induced uniaxial anisotropy, and no higher symmetry orders, in principle only a rectangular lattice can induce anisotropy through interactions: a square or hexagonal lattice of interacting, uniformly magnetized particles should be isotropic. Nevertheless, Mathieu *et al* [40] have reported experimentally a *four-fold* anisotropy in a sample of interacting circular magnetic dots arranged on a square lattice. They explained this as being due to deviations from the perfect uniformly magnetized state of each particle. This is very interesting because it is the interacting analogy to *configurational anisotropy*: a higher-order anisotropy appears because of first and higher spatial order terms in the magnetization field. In this case, however, the non-uniformity couples to the geometry of the *lattice* instead of to the geometry of the *motif* as occurs in configurational anisotropy.

5. Conclusion

We have presented a review of an extensive study which we have performed into the influence of shape and size on the magnetic properties of nanostructures. We have shown that shape plays an essential role in determining magnetic properties, on the one hand by inducing anisotropy and on the other hand by stabilizing/destabilizing the single domain state. We have shown the key role played by small deviations from uniformity in the magnetization field within the nanostructures. These small deviations allow the shape of the nanomagnets themselves and the shape of the lattice on which they are arranged to couple into the magnetic energy surface, causing unexpected higher-order anisotropy terms to appear which can dominate the magnetic properties. Equally important is the competition which exists between the quantum mechanical exchange energy and the classical magnetostatic energy. This not only determines whether a nanostructure will exhibit a single domain state, but also controls the magnetization deviations which allow the coupling between (non-elongated) shape and magnetism. Understanding these things opens the way to designing new nanostructured magnetic materials where the magnetic properties can be tailored to a particular application with a very high degree of precision.

Acknowledgments

This work would not have been possible without the excellent assistance of my colleagues, Professor M E Welland, Dr A O Adeyeye and D K Koltsov. Much of the work described in this paper was funded by the UK Royal Society. The author is supported by St John's College, Cambridge.

Appendix

A.1. Proof that the anisotropy field has the same magnitude and symmetry as $E''(\phi)/M_s$

Suppose that the anisotropic energy density of a magnet can be described by the function $E(\phi)$ where ϕ is the magnetization direction. The anisotropy *field* H_a is defined as the magnetic field which would need to be applied to the magnet in the direction ϕ in order to give the same energy profile as the function $E(\phi)$ for small deviations of the magnetization about ϕ. Let the size of any deviations of the magnetization direction from ϕ be described by the variable θ. In this case, the Zeeman energy expression gives

$$E = \text{constant} - MH_a\cos\theta \tag{5}$$

and hence

$$\frac{\mathrm{d}E}{\mathrm{d}\theta} = MH_a\theta \qquad \text{in the limit of small } \theta. \tag{6}$$

Differentiating with respect to θ once more gives

$$\frac{\mathrm{d}^2E}{\mathrm{d}\theta^2} = MH_a. \tag{7}$$

Since θ is simply the deviation in ϕ, the identity $\mathrm{d}\theta = \mathrm{d}\phi$ can be made and hence

$$H_a = \frac{1}{M_s}E''(\phi). \tag{8}$$

A.2. Proof that anisotropy energy and anisotropy field are related by $U = 2M_sVH_a/n^2$

A magnet with an anisotropy of rotational symmetry order n will have a dependence of energy U on the magnetization direction ϕ, which can be described by

$$U(\phi) = A_nK_n\cos^2\frac{n\phi}{2} \tag{9}$$

where A_n is a scaling constant and K_n is the anisotropy constant. Differentiating this expression twice with respect to ϕ gives

$$\frac{\mathrm{d}^2U(\phi)}{\mathrm{d}\phi^2} = \frac{-n^2A_nK_n}{2}\cos n\phi. \tag{10}$$

The energy *density* E can then be found by dividing the energy by the volume of the magnet V to give

$$\frac{\mathrm{d}^2E(\phi)}{\mathrm{d}\phi^2} = \frac{-n^2A_nK_n}{2V}\cos n\phi. \tag{11}$$

Substituting (11) into (8) then gives

$$H_a(\phi) = -\frac{n^2A_nK_n}{2M_sV}\cos n\phi. \tag{12}$$

Comparing the magnitudes of the trigonometric functions of (12) and (9) then gives the desired relationship

$$U = \frac{2M_sH_aV}{n^2}. \tag{13}$$

References

[1] White R L, New R M H and Pease R F W 1997 *IEEE Trans. Magn.* **33** 990

[2] Moore G E 1975 *Int. Electronic Devices Meeting (IEDM) (Technical Digest vol 75)* (Piscataway, NJ: IEEE) p 11

[3] Landau L and Lifschitz E 1935 *Physik. Z. Sowjetunion* **8** 153
Brown W F 1963 *Micromagnetics* (New York: Wiley)
Aharoni A 1996 *Introduction to the Theory of Ferromagnetism* (Oxford: Oxford University Press)

[4] Cowburn R P and Welland M.E 1999 *J. Appl. Phys.* **86** 1035

[5] Prinz G A 1998 *Science* **282** 1660

[6] Hammar P R, Bennett B R, Yang M J and Johnson M 1999 *Phys. Rev. Lett.* **83** 203

[7] DiVincenzo D D 1997 *J. Appl. Phys.* **81** 4602

[8] Prutton M 1964 *Thin Ferromagnetic Films* (London: Butterworth)
Chikazumi S 1964 *Physics of Magnetism* (New York: Wiley)

[9] Bland J A C and Heinrich B (eds) 1994 *Ultrathin Magnetic Structures* (Berlin: Springer)

[10] Parkin S S P, More N and Roche K P 1990 *Phys. Rev. Lett.* **64** 2304

[11] Baibich M N, Broto J M, Fert A, van Dau F N, Petroff F, Etienne P, Creuzet G, Friederich A and Chazelas J 1988 *Phys. Rev. Lett.* **61** 2472
Binasch G, Grunberg P, Saurenbach F and Zinn W 1989 *Phys. Rev.* B **39** 4828

[12] Gay J G and Richter R 1986 *Phys. Rev. Lett.* **56** 2728
Jonker B T, Walker K-H, Kisker E, Prinz G A and Carbone C 1986 *Phys. Rev. Lett.* **57** 142

[13] Fasol G 1998 *Science* **280** 545 and references therein

[14] Portier X and Petford-Long A K 1999 *J. Phys. D: Appl. Phys.* **32** R89

[15] Kirk K J, Chapman J N and Wilkinson C D W 1999 *J. Appl. Phys.* **85** 5237
Gomez R D, Luu T V, Pak A O, Kirk K J and Chapman J N 1999 *J. Appl. Phys.* **85** 6163
Kirk K J, Chapman J N and Wilkinson C D W 1997 *Appl. Phys. Lett.* **71** 539
McVitie S and Chapman J N 1997 *Microscopy Microanal.* **3** 146
Pohm A V, Anderson J M, Beech R S and Daughton J M 1999 *J. Appl. Phys.* **85** 4771
Everitt B A, Pohm A V, Beech R S, Fink A and Daughton J M 1998 *IEEE Trans. Magn.* **34** 1060
Everitt B A, Pohm A V and Daughton J M 1997 *J. Appl. Phys.* **81** 4020
Lu Y *et al* 1999 *J. Appl. Phys.* **85** 5267
Lu Y, Altman R A, Marley A, Rishton S A, Trouilloud P L, Xiao G, Gallagher W J and Parkin S S P 1997 *Appl. Phys. Lett.* **70** 2610
Koch R H, Deak J G, Abraham D W, Trouilloud P L, Altman R A, Lu Y, Gallagher W J, Scheuerlein R E, Roche K P and Parkin S S P 1998 *Phys. Rev. Lett.* **81** 4512
Kong L, Pan Q, Cui B, Li M and Chou S Y 1999 *J. Appl. Phys.* **85** 5492

[16] Schrefl T, Fidler J, Kirk K J and Chapman J N 1999 *J. Appl. Phys.* **85** 6169
Schrefl T, Fidler J, Kirk K J and Chapman J N 1997 *J. Magn. Magn. Mater.* **175** 193
Oti J O and Russek S E 1997 *IEEE Trans. Magn.* **33** 3298
Shi J, Zhu T, Durlam M, Chen E, Tehrani S, Zheng Y F and Zhu J G 1998 *IEEE Trans. Magn.* **34** 997
Gadbois J, Zhu J G, Vavra W and Hurst A 1998 *IEEE Trans. Magn.* **34** 1066

[17] Jamet J P *et al* 1998 *Phys. Rev.* B **57** 14 320
Hehn M, Ounadjela K, Bucher J P, Rousseaux F, Decanini D, Bartenlian B and Chappert C 1996 *Science* **272** 1782
Hehn M, Ounadjela K, Ferre R, Grange W and Rousseaux F 1997 *Appl. Phys. Lett.* **71** 2833
Wirth S, von Molnar S, Field M and Awschalom D D 1999 *J. Appl. Phys.* **85** 5249
Shi J, Awschalom D D, Petroff P M and Babcock K 1997 *J. Appl. Phys.* **81** 4331
Gider S, Shi J, Awschalom D D, Hopkins P F, Campman K L, Gossard A C, Kent A D and von Molnar S 1996 *Appl. Phys. Lett.* **69** 3269
Wirth S, Heremans J J, von Molnar S, Field M, Campman K L, Gossard A C and Awschalom D D 1998 *IEEE Trans. Magn.* **34** 1105
Stamm C, Marty F, Vaterlaus A, Weich V, Egger S, Maier U, Ramsperger U, Fuhrmann H and Pescia D 1998 *Science* **282** 449
Savas T A, Farhoud M, Smith H I, Hwang M and Ross C A 1999 *J. Appl. Phys.* **85** 6160
Thielen M, Kirsch S, Weinforth H, Carl A and Wassermann E F 1998 *IEEE Trans. Magn.* **34** 1009
Wassermann E F, Thielen M, Kirsch S, Pollmann A, Weinforth H and Carl A 1998 *J. Appl. Phys.* **83** 1753

Kleiber M, Kummerlen F, Lohndorf M, Wadas A, Weiss D and Wiesendanger R 1998 *Phys. Rev.* B **58** 5563
Meier G, Kleiber M, Grundler D, Heitmann D and Wiesendanger R 1998 *Appl. Phys. Lett.* **72** 2168
[18] Marty F, Vaterlaus A, Weich V, Stamm C, Maier U and Pescia D 1999 *J. Appl. Phys.* **85** 6166
Aign T *et al* 1998 *Phys. Rev. Lett.* **81** 5656
Gu E, Ahmad E, Gray S J, Daboo C, Bland J A C, Brown L M, Ruhrig M, McGibbon A J and Chapman J N 1997 *Phys. Rev. Lett.* **78** 1158
[19] Broers A N 1995 *Phil. Trans. R. Soc.* A **353** 291
[20] Smith N, Markham D and LaTourette D 1989 *J. Appl. Phys.* **65** 4362
[21] Cowburn R P, Koltsov D K, Adeyeye A O and Welland M E 1998 *Appl. Phys. Lett.* **73** 3947
[22] Kerr J 1877 *Phil. Mag.* **3** 339
[23] Cowburn R P, Adeyeye A O and Welland M E 1998 *Phys. Rev. Lett.* **81** 5414
[24] Cowburn R P, Ercole A, Gray S J and Bland J A C 1997 *J. Appl. Phys.* **81** 6879
[25] Cowburn R P and Welland M E 1998 *Phys. Rev.* B **58** 9217
[26] Ryan J M, Hoole A C F and Broers A N 1995 *J. Vac. Sci. Technol.* B **13** 3035
[27] Chang T H P *et al* 1988 *IBM J. Res. Dev.* **32** 462
[28] Gadbois J, Zhu J G, Vavra W and Hurst A 1998 *IEEE Trans. Magn.* **34** 1066
[29] Cowburn R P, Koltsov D K, Adeyeye A O and Welland M E 1999 *Europhys. Lett.* **48** 221
[30] Bean C P 1955 *J. Appl. Phys.* **26** 1381
[31] Schabes M E and Bertram H N 1988 *J. Appl. Phys.* **64** 1347
[32] Cowburn R P and Welland M E 1998 *Appl. Phys. Lett.* **72** 2041
[33] Brown W F Jr 1968 *J. Appl. Phys.* **39** 993
[34] Cowburn R P, Koltsov D K, Adeyeye A O, Welland M E and Tricker D M 1999 *Phys. Rev. Lett.* **83** 1042
[35] Dunin-Borkowski R E, McCartney M R, Kardynal B and Smith D J 1998 *J. Appl. Phys.* **84** 374
[36] Stoner E C and Wohlfarth E P 1948 *Phil. Trans. R. Soc.* A **240** 74
[37] Cowburn R P, Adeyeye A O and Welland M E 1999 *New J. Phys.* **1** 16
[38] Chapman J N, Johnston A B, Heyderman L J, McVitie S, Nicholson W A P and Bormans B 1994 *IEEE Trans. Magn.* **30** 4479
[39] Allenspach R 1994 *Phys. World* **7** 44
[40] Mathieu C *et al* 1997 *Appl. Phys. Lett.* **70** 2912